


Suppression of wear in dry sliding friction induced by negative thermal expansionAleksandr S. Grigoriev ^{*}, Evgeny V. Shilko , Andrey I. Dmitriev , and Sergey Yu. Tarasov 
Institute of Strength Physics and Materials Science SB RAS, Tomsk 634055, Russia (Received 15 May 2020; revised 25 August 2020; accepted 25 September 2020; published 16 October 2020)

Surface temperature is among crucial factors which control wear during sliding dry contact. Using computer modeling, we study the possibility to achieve close to zero rate of surface wear during sliding friction of the special type of materials which possess negative thermal expansion. The numerical simulations reveal two wear regimes for materials with negative thermal expansion coefficient as dependent on the applied normal stress level. When the applied stress is lower than that of a critical level, a steady almost zero wear rate and nanorough surface are achieved during friction. Otherwise, wear rate is of the same order of magnitude as for “traditional” materials with positive thermal expansion coefficient. The critical stress value is analyzed depending on the material’s mechanical, thermophysical, and surface roughness characteristics.

DOI: [10.1103/PhysRevE.102.042801](https://doi.org/10.1103/PhysRevE.102.042801)**I. INTRODUCTION**

Temperature is a fundamental factor to control friction and wear in a solid-solid contact at all scales. The locality of energy dissipation in rubbing between rough surfaces results in the fact that the mean subsurface layer temperature may be much higher than that of the bulk of the body and, moreover, the so-called flash can be higher than 1000 K [1–7]. Temperature dependencies of mechanical characteristics, acceleration of phase transformations and mechanochemical reactions, activation of special thermolubrication mechanisms, as well as some other phenomena determine the evolution and dynamics of wear and friction parameters at elevated subsurface temperatures [8–13]. Both individually and in the aggregate these factors may dramatically change the wear and friction evolution of the solid body especially if coexisting within the same temperature and contact stress ranges. However, there is a phenomenon that is manifested on a majority of materials at elevated temperatures. It is thermal expansion.

Control of thermal expansion is among the most important fundamental problems in friction physics but can be difficult to achieve. Actually, the majority of both natural and artificial materials possess a positive thermal expansion coefficient (TEC), whose magnitudes vary in the range $\alpha \sim 10^{-6} - 10^{-5} \text{ K}^{-1}$. The positive thermal expansion (PTE) is a critical issue in many applications when a material experiences intense heating—aerospace engineering, electronics, etc. [14]. It is an especially important factor for extremely localized deformation and energy dissipation, i.e., in sliding friction conditions when two rough surfaces are contacting each other only by real contact areas and the intense heating results in additional (thermal-induced) stress between contacting and thermally expanding asperities.

These thermal-induced stresses have at least two negative effects on the sliding friction. The first is that these stresses

facilitate reaching the local critical stress values and thus promote either inelastic deformation or fracture of the asperity. Second, these stresses provide the effect of surface separation which, even if a negligible macroscopic value, serves for reducing the number of contact spots and stress concentration on those left. The latter also leads to a fracture of contacting asperities. An integral effect of PTE is a wear rate growth and feasibility of a thermoelastic instability, the most general and intriguing type of instabilities during friction [15,16]. This term has been proposed by Barber [17], who was first to indicate that the self-supporting process of frictional heating of the surface may result in the total annihilation of the initial asperities and uncontrolled growth of wear and friction force (catastrophic wear).

A traditional solution to this fundamental problem is related either with selecting optimum external factor values (load, speed, contact geometry, lubrication, etc.) in order to reduce the contact stress or with applying special materials with heat- and wear-resistant stable structures and phase composition that provide the stability of distribution of contact spots [10,18,19]. A promising alternative approach is applying new adaptive materials, which possess a negative thermal expansion (NTE) coefficient. Over the past decade, the materials were developed which reveal structural adaptation and provide contraction under heating [20–25] as well as different NTE performance temperature intervals.

The most attractive materials to be used in sliding couples should possess high mechanical characteristics, thermal stability, and negative thermal expansion ability in a wide temperature range spanning from ambient temperatures to hundreds and even above a thousand K. These requirements can be satisfied using ceramic materials synthesized of oxides, nitrides, etc., whose negative values of thermal expansion coefficient originate from unusual topology of the structure exhibiting a network of rigid unit modes (units) connected by relatively soft linkages. The most known examples are oxides with semirigid polyhedra and rigid bonds, including families of materials based on the ZrV_2O_7 , ZrW_2O_8 , $\text{Sc}_2\text{W}_3\text{O}_{12}$, and

^{*}Corresponding author: grigoriev@ispms.ru

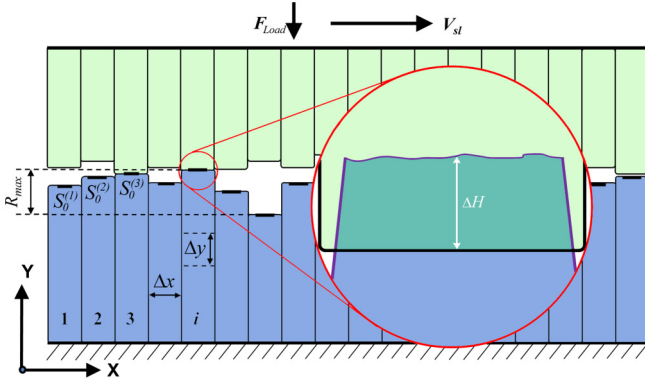


FIG. 1. Schematic diagram of sliding contact between rigid (top) and deformable (bottom) surfaces.

$\text{NaZr}_2(\text{PO}_4)_3$ structures, as well as siliceous AST zeolites. An extensive list of the NTE materials with corresponding NTE effect and thermal stability temperature ranges can be found in recent reviews [26,27]. At least some of these materials possessing wide enough NTE temperature intervals as well as high thermal expansion coefficient and elastic moduli values (for instance, zirconium tungstate ZrW_2O_8 with $\alpha \approx -3 \times 10^{-5} \text{ K}^{-1}$ [14,20,28] and Young's modulus $E \approx 10^2 \text{ GPa}$ [29,30]) are the most promising for being used to stabilize friction and wear.

It is suggested that using the NTE effect in sliding may reduce scatter of asperity heights due to thermal-induced contraction and, therefore, result in more uniform load distribution as well as wear rate reduction. This brings us to the feasibility of “wearless sliding friction,” i.e., sliding friction characterized by very mild or even zero wear at rather high sliding speeds and normal load. It is understandable that a truly wearless sliding friction regime is possible only in the case of zero adhesion between the surfaces.

In our work, we introduce a theoretical study of the unlubricated wear of rough surfaces of NTE materials. We focus on revealing conditions under which thermal-induced contraction of asperities makes it possible to almost completely suppress the wear. To carry out the study, we developed a microscale asperity-based model of sliding friction of a model NTE material with an absolutely rigid counterbody. Such a radical problem formulation implies that the friction energy dissipation occurs exclusively in a subsurface layer of NTE material so that the NTE effect on thermoelastic instability as well as friction and wear dynamics could be unambiguously evaluated.

II. MODEL

The rough surface of NTE material was modeled by a number of independently deformable asperities so that each of them was characterized by the Y position of the top and some parameter called here effective contact surface area S (Fig. 1).

An instantaneous real contact area between asperities belonging to opposite surfaces is determined by plenty of factors and continuously changes during sliding [31–33]. Therefore, S parameter could be defined as an effective parameter to

characterize the time-average value of instantaneous real contact areas arising between two asperities belonging to opposite surfaces. For simplicity we assume that S is the individual geometry characteristic of each deformable asperity, i.e., it is independent of the opposing contacting rigid asperity choice. Such a simplification has only a negligible effect on the final results and corresponds to the case when the rigid body asperities are flat-top (Fig. 1). Initial values of the asperity's top position $Y_0^{(i)}$ and contact areas $S_0^{(i)}$, where i is the asperity number, were drawn at random from homogeneous distributions at specified intervals $[Y_0^{\min}, Y_0^{\max}]$ and $[S_0^{\min}, S_0^{\max}]$, respectively. The roughness of the rigid countersurface was set similarly.

The surfaces were characterized by roughness parameters $R_{\max} = (Y_0^{\max} - Y_0^{\min})$ and $R_a = 1/m \sum_{i=1}^m |Y_0^{(i)} - Y_{\text{mean}}|$, where m is the number of asperities in the model and $Y_{\text{mean}} = 1/m \sum_{i=1}^m Y_0^{(i)}$ is the mean asperity height. The asperity width Δx was equal for all the asperities of both surfaces.

Sliding friction interaction between deformable and rigid asperities involves both normal F_N and tangential F_t forces. Normal force F_N provides compression of the deformable asperity by the rigid one and for simplicity reasons, it was determined using the spring stiffness K approximation

$$F_N = K \Delta H = K_{\min} \frac{S_0}{S_0^{\min}} \Delta H, \quad (1)$$

where $\Delta H = Y - Y_0$ is the asperity height reduction by compression and K_{\min} is the stiffness of the minimum contact area S_0^{\min} asperity. Here, we assume that asperity stiffness K depends only on the asperity contact area. It is known from the solution of the problem of semi-infinite plate edge loaded by a point force that both elastic stresses and strains slowly fall off with the distance away from the force application point. The effect of the asperity height on the compression resistance is, therefore, assumed as negligible and ignored.

The tangential asperity interaction force was determined as $F_t = \mu F_N$ where μ is the local coefficient of friction kept constant for all contacts. Assuming that almost all mechanical energy dissipated during sliding friction transforms into heat, friction heat release power in the contact of two asperities was calculated from the friction force F_t and sliding speed V_{sl} : $q = \mu F_N V_{sl}$. Heat removal from each asperity to the bulk of the deformable body was calculated by means of numerically solving the one-dimensional heat conductivity problem:

$$\frac{\partial T}{\partial t} = a \frac{\partial^2 T}{\partial y^2}, \quad (2)$$

where $a = k/(c\rho)$ is the thermal diffusivity, k is the heat conductivity, c is the specific heat capacity, and ρ is the density. A heat source q and constant temperature $T = T_0$ were used as boundary conditions on opposite ends of the asperity. A solution to the heat conductivity equation was obtained using the finite difference method with a step Δy numerically equal to asperity width Δx . Here, we assume that the temperature of the asperity is associated with the temperature of the top cell. Heat transfer along the X axis was ignored.

Thermal expansion leads to changing the surface roughness topography. It was assumed that since deeper surface layers are under constrain conditions and deform consistently

then the temperature-induced change of the asperity height (Y coordinate of the top of asperity) is almost totally determined by thermal expansion of the top cell:

$$Y = Y_0 + \alpha \Delta T \Delta y, \quad (3)$$

where $\Delta T = T - T_0$ is the asperity temperature difference between its current (T) and initial (T_0) values and α is the thermal expansion coefficient. Thermal expansion of the asperity also results in changing the effective contact area as follows:

$$S = S_0(1 + \alpha \Delta T)^2. \quad (4)$$

The value of equivalent stress in asperity of the deformable body was used as a criterion of asperity wear. The meaning of such a criterion is similar to that of commonly used von Mises stress criterion:

$$\sigma_{\text{eq}} = \frac{1}{\sqrt{2}} \sqrt{2\sigma_N^2 + 6\sigma_\tau^2} = \frac{F_N}{S} \sqrt{1 + 3\mu^2} \geq C, \quad (5)$$

where $\sigma_N = F_N/S$, $\sigma_\tau = F_\tau/S$, and C is the material strength characteristic. When inequality in the right part of (5) becomes true for some asperity, i.e., the criterion is fulfilled, then its height (Y coordinate of the top) is reduced by quantity dH_w . The corresponding wear volume may be estimated as $dW_{\text{asp}} = dH_w S_0$. We assume that the asperity wear act does not change the corresponding values of S_0 , T , and K .

The ‘‘elementary’’ wear volume dH_w can vary widely since it depends on the majority of factors including wear mechanisms: mild wear, pulling out, fragmentation, etc. [34–40]. Generally, the wear mechanism is determined by the contact pressure. Consequently, the worn material volume per elementary wear act H_w is determined both by the ductility (or brittleness) ratio of the material and the applied stress level. Here, we assume simple linear dependence of the elementary wear dH_w on equivalent stress σ_{eq} achieved on the contact area:

$$H_w = H_w^{\min} + \frac{dH_w}{d\sigma_{\text{eq}}} (\sigma_{\text{eq}} - C), \quad (6)$$

where $dH_w/d\sigma_{\text{eq}} = \text{const}$ and H_w^{\min} is the asperity minimum wear volume at $\sigma_{\text{eq}} = C$.

Sliding friction was modeled by discretely moving the rigid counterbody over the surface of a damageable one along the X axis at a constant sliding speed V_{sl} (Fig. 1). The time interval between two successive displacement acts $\Delta t = \Delta x/V_{\text{sl}}$ corresponded to the contact dwell time when frictional heat was released. The displacement step size was equal to the asperity width Δx so that the whole system of asperity contacts was fully modified. No dynamic sliding effects including elastic wave propagation on the surface and in the bulk of the bodies were considered within this model. It was assumed that the system is under force equilibrium condition during each moment of time (it is a so-called ‘‘overdamped’’ system): $F_{\text{Load}} = \sum_{i=1}^m F_N^{(i)}$, where F_{Load} is applied normal force and $F_N^{(i)}$ is the reaction force (1) from the i asperity. Following this assumption, we determine the equilibrium Y position of the rigid body surface with respect to deformable one at each time interval between successive displacement acts. The total wear was characterized using $W(t)$ dependencies, where $W = \sum_{t=0}^{n\Delta t} \sum_{i=1}^m H_w^{(i)} S_0^{(i)}$ is the wear debris volume and n is the current time step number. It is assumed that wear debris is

fully removed from the worn surface and thus has no effect on the further course of surface interaction. The sliding friction process stability was estimated from analyzing the $W(t)$ dependencies for different contact stress levels. It is reasonable that steady sliding may be characterized by a close to constant mild wear rate estimated as the mean value of the $w = dW/dt$ derivative. On the contrary, instable (catastrophic) wear would be characterized by $w > 0$. Also, the time stability of the wear process would be imprinted on the worn surface topography.

We treated a deformable body model material, which possesses negative TEC: thermal expansion coefficient $\alpha = -8.5 \times 10^{-5} \text{ K}^{-1}$, density $\rho = 9000 \text{ kg/m}^3$, heat capacity $c = 380 \text{ J/(kg K)}$, heat conductivity $k = 5 \text{ W/(m K)}$, Young’s modulus $E = 125 \text{ GPa}$, the strength of asperity material $C = 4 \text{ GPa}$. The damageable and rigid surfaces were characterized by roughness $R_{\text{max}} \approx 2 \mu\text{m}$, $R_a \approx 0.5 \mu\text{m}$, and $R_{\text{max}}^{\text{rigid}} \approx 0.5 \mu\text{m}$, $R_a^{\text{rigid}} \approx 0.125 \mu\text{m}$, respectively. The following parameters of asperity friction and wear were used: minimum elementary wear volume $H_w^{\min} = 0.4 \mu\text{m}$, $dH_w/d\sigma_{\text{eq}} = 10^{-16} \text{ m/Pa}$, and local coefficient of friction $\mu = 0.1$. The values shown above correspond to the characteristics of ceramic materials (including promising NTE ceramic materials) and typical surfaces in order of magnitude.

III. RESULTS

Intense heating and wear of asperities is accompanied by establishing the constant levels of mean wear rate w and subsurface temperature. The absolute value of w is determined by the number of contact spots on which critical contact pressure $\sigma_N \geq C/\sqrt{1 + 3\mu^2}$ is achieved. The applied normal stress $\sigma_{\text{Load}} = F_{\text{Load}}/(m\Delta x^2)$ is, therefore, a key factor to determine the wear rate under tangential contacting.

The main fundamental result obtained on the NTE model material is the threshold nature of the $w(\sigma_{\text{Load}})$ dependency, i.e., there is some threshold value (σ_{crit}) of applied normal stress σ_{Load} above which there occurs a transition from steady low wear ($w \rightarrow 0$) to catastrophic ($w > 0$) wear. The wear evolution on NTE model material is represented in Fig. 2(a) as $W(t)$ dependencies plotted for different applied normal stresses. All curves demonstrate a short-time running-in stage when the wear rate decreases from the maximum initial value to a low steady value determined by σ_{Load} . The $W(t)$ curves may be divided into two sets. The first set was obtained at $\sigma_{\text{Load}} < \sigma_{\text{crit}}$ and these curves demonstrate a steady low wear regime of sliding (or ‘‘wearless friction’’). The second set of curves relate to $\sigma_{\text{Load}} > \sigma_{\text{crit}}$ and their running-in stages give way to the increasing wear stage, which is commonly observed in dry friction on the PTE materials in the absence of any wear reduction mechanisms. Indeed, a similar study for PTE material with the same physical properties but TEC of the opposite sign ($\alpha = 8, 5 \times 10^{-5}$) showed the absence of the wearless friction stage [Fig. 2(b)]. The steady wear stage is observed for all $\sigma_{\text{Load}} > 0$ so that the mean wear rate is monotonically increased from mild to catastrophic level with the σ_{Load} .

Initially, the damageable surface is rather rough (Fig. 3) and it becomes smoother in the process of sliding. The steady low wear friction for the model NTE material is characterized

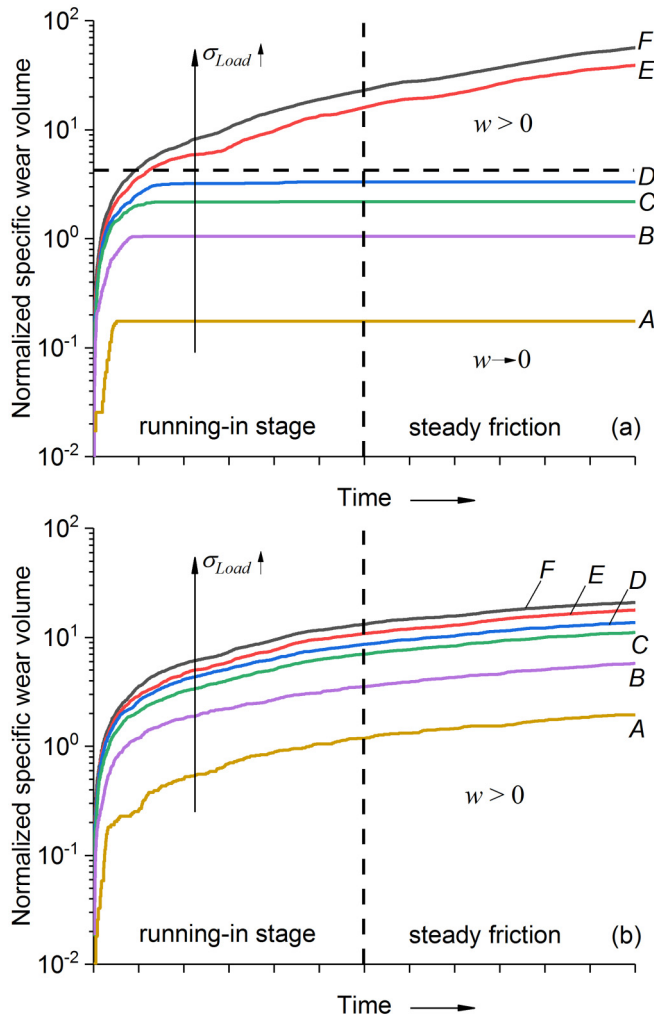


FIG. 2. Wear vs time curves for NTE (a) and PTE (b) model materials tested at different applied normal stress levels $\sigma_{Load}/\sigma_{crit}$: 0.3 (A), 0.6 (B), 0.9 (C), 0.98 (D), 1.1 (E), 1.2 (F). The worn volume is shown here in dimensionless specific (per asperity) units $W' = W/(mH_w^{min}S_0^{max})$. Horizontal dashed line is a boundary between low wear and catastrophic wear stages. Vertical dashed line conditionally separates the running-in and steady friction stages.

by one order of magnitude lower roughness of the worn surface [Fig. 4(a)]. Qualitatively different two-scale topography of the worn surface is observed for the catastrophic wear regime [Fig. 4(b)]. The main corrugation is characterized by periodic stepped profile (0.467 μm mean height and 178 μm mean width in the present case). The profile steps appear by means of successive shaving the deformable surface asperities by those of the rigid countersurface. Such a shaving provides a wear rate even higher than that achieved on a PTE at the same values of σ_{Load} (Fig. 2). A lower order of magnitude roughness may be discovered on the profile step surfaces,

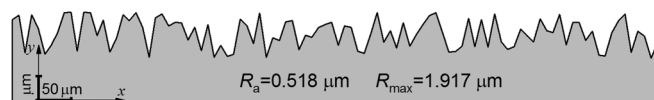


FIG. 3. The initial surface topography.

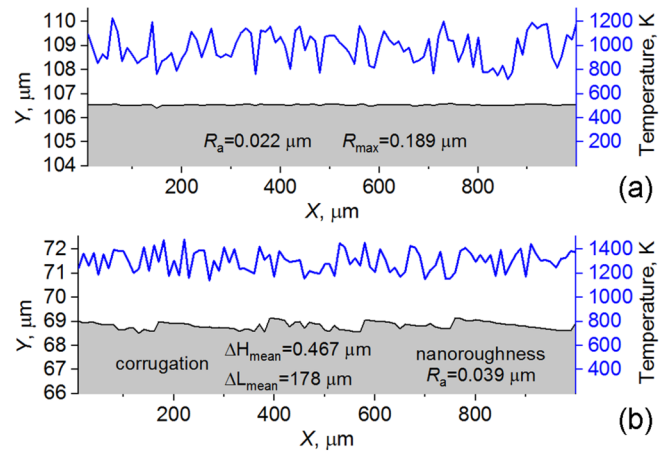


FIG. 4. The worn surfaces and temperature profiles (blue curves) of NTE model material: (a) steady low wear mode at $\sigma_{Load} < \sigma_{crit}$; (b) catastrophic wear mode at $\sigma_{Load} > \sigma_{crit}$. See Supplemental Material videos [41].

whose parameters are comparable with those obtained at the steady low wear stage.

The PTE model material worn surfaces demonstrate only one type of topography whose roughness slowly increases with the applied contact pressure, for example twice increase in applied normal stress leads to only 10% increase in R_a [Figs. 5(a) and 5(b)].

The difference between the two worn surface topographies obtained on the NTE material [Figs. 4(a) and 4(b)] is explained by the temperature-induced shrinking of the asperity dimensions including height and effective contact area. Since surfaces are rough then local contact stresses $\sigma_N^{(i)}$ are distributed inhomogeneously and the most heavily loaded contact areas experience the highest frictional heating, i.e., maximum thermal shrinking. Although the effect of thermally induced reduction of roughness is in the order of several percent, at least this is true at $\sigma_{Load} < \sigma_{crit}$, it serves for

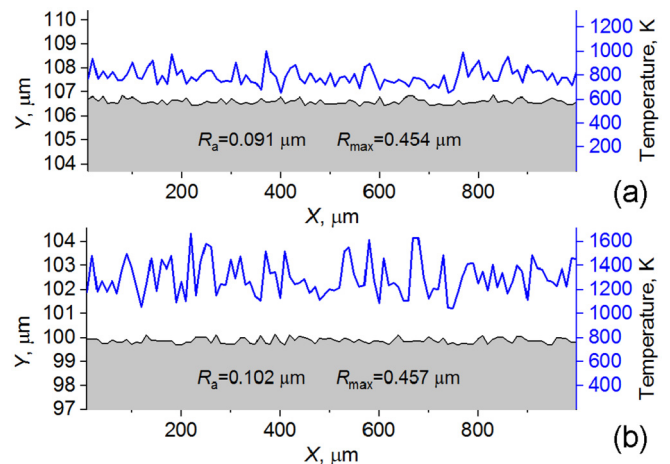


FIG. 5. The worn surfaces and temperature profiles (blue curves) of model PTE material. Both cases correspond to catastrophic wear mode at $\sigma_{Load} = 0.6\sigma_{crit}$ (a) and $\sigma_{Load} = 1.4\sigma_{crit}$ (b). See Supplemental Material videos [41].

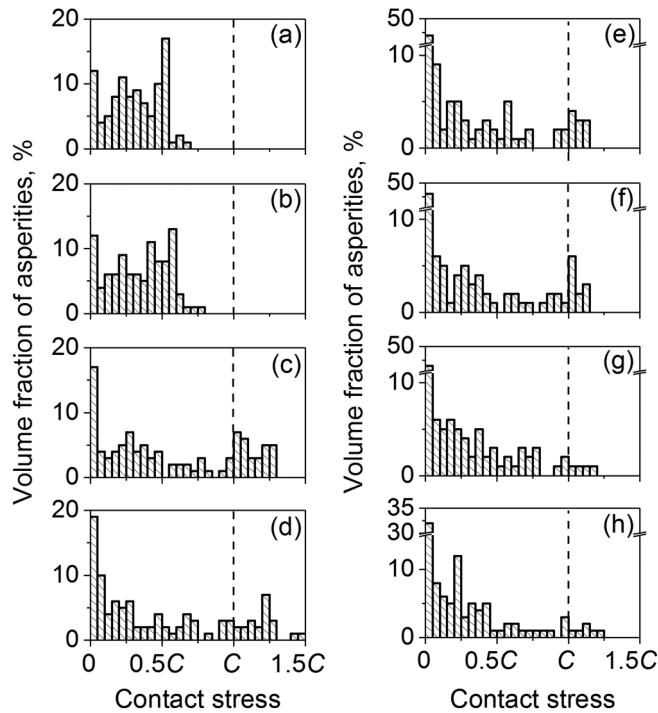


FIG. 6. Contact stress distribution histograms for NTE (a)–(d) and PTE (e)–(h) model materials at different applied contact pressure level σ_{Load} : (a), (e) $0.9\sigma_{crit}$; (b), (f) $0.98\sigma_{crit}$; (c), (g) $1.1\sigma_{crit}$; (d), (h) $1.2\sigma_{crit}$.

efficient redistributing of the load on previously less loaded asperities so that the maximum contact stresses reduce too and stress distribution becomes more homogeneous.

The contact stress distribution histograms in Figs. 6(a) and 6(b) show that when $\sigma_{Load} < \sigma_{crit}$, the maximum stresses stay below the asperity material strength C and this is the condition for steady low wear sliding with only sporadic and local wear peaks originating from the sporadic nature of asperity height distribution. These peaks provide a low but finite value of wear rate, which however stays close to zero.

When $\sigma_{Load} > \sigma_{crit}$ there is always a fraction of asperities with the contact stresses above the ultimate stress C [Figs. 6(c) and 6(d)]. The higher the applied contact pressure, the higher is the asperity fraction with the contact stress at the level of the material’s strength. This may be a rationale behind the ever-increasing wear and specific type of the worn surface topography [Fig. 4(b)]. It was shown by means of parametric study that both the height and width of the corrugation are unambiguously related to the applied normal stress σ_{Load} . The higher the σ_{Load} , the higher is the fraction of rigid asperities that dig into the opposing surface and then cut shorter chips thus leaving the shorter marks on it.

The histograms in Figs. 6(e)–6(h) for PTE materials testify that for all $\sigma_{Load} > 0$ there is always a fraction of asperities with contact stresses above the material strength. This results from thermal elongation of the PTE asperities, which facilitates stress concentration on the highest ones and their ensuing wear even at low applied pressure levels.

The thermally induced origin of the above-described contact pressure and wear behaviors may be illustrated by means

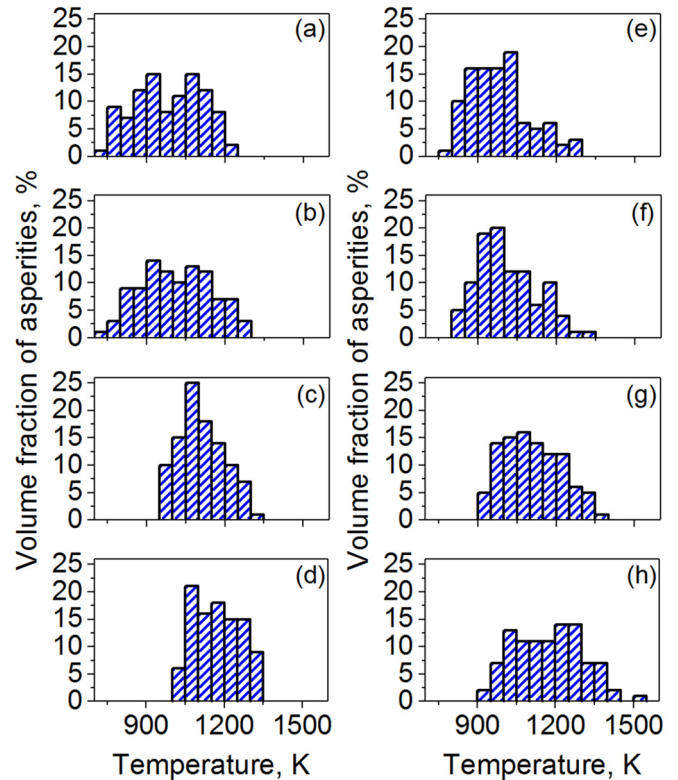


FIG. 7. Temperature distribution histograms for NTE (a)–(d) and PTE (e)–(h) model materials at different applied contact pressure level σ_{Load} : (a), (e) $0.9\sigma_{crit}$; (b), (f) $0.98\sigma_{crit}$; (c), (g) $1.1\sigma_{crit}$; (d), (h) $1.2\sigma_{crit}$.

of characteristic temperature distributions of the deformable body asperities established at the steady sliding stage (see the blue curves in Figs. 4 and 5). Despite the fact that the details of the temperature profile change in time, integral characteristics of the temperature distribution stay invariable during the steady sliding stage. Figure 7 shows the worn surface temperature distribution histograms obtained for different normal loads. When comparing these histograms for the NTE material [Figs. 7(a)–7(d)] one can see that temperature scatter decreases by a factor of 2 after crossover from the low to catastrophic wear regime while mean surface temperature monotonically grows with σ_{Load} . Such a decrease may be explained by the fact that each asperity periodically acts like a normal stress concentrator due to wear of other ones and experiences frictional heating and wear with the ensuing temporal contact stress reduction. Consequently, all asperities experience almost equal integral heating and the asperity’s temperature scatter is a relatively small percentage [within the 20% of the mean surface heating as shown in Fig. 4(b) and Figs. 7(c) and 7(d)]. At the same time, during the low wear regime of friction [Figs. 4(a), 7(a), and 7(b)], the asperities suffer practically no wear so that the worn surface roughness is changed very slowly. The highest asperities more often contact with those of the rigid countersurface therewith, so that their temperatures become essentially higher than those of the less high ones. As noted above, this intensive heating of the highest asperities serves to level the worn surface. Simultaneously, the asperities cool down by means of heat

removal to the underlying material layers and thus increase their heights. Competing processes of frictional heating and heat removal cooling determines height dependence of the local asperity temperatures and, consequently, their wider scatter from the mean value as compared to that of the catastrophic wear regime [$>40\%$ of the mean worn surface temperature in Fig. 4(a)]. Let us note that the greater asperity temperature scatter in sliding is a necessary factor for maintaining a nanoscale roughness at the level of roughness established at the running-in stage as well as for manifestation of a low wear regime.

Completely other behavior is observed for PTE material [Figs. 5 and 7(e)–7(h)] when both mean worn surface temperature and local temperature scatter grow in proportion to the normal load. The rationale behind such a fact is that the highest asperities mainly contact those of the rigid counter-surface and therefore are heated to high temperatures since they increase their heights with the temperature so that contact stress is localized on them. Wear of those highest and high-temperature heated asperities can only partially reduce this normal stress localization effect, which is a physical reason behind the effect of thermoelastic instability theoretically considered by Barber.

IV. DISCUSSION

The results obtained in this work show that thermal shrinking of the worn surface asperities can be a factor to reduce the roughness down to the nanoscale and complete changing of the wear regime for materials with negative thermal expansion coefficient. In addition, a row of questions arises as to the effects of initial roughness parameters of both surfaces, specifics of the thermally induced changing of the asperity contact area, as well as mechanical and thermal-physical characteristics of the NTE material on the occurrence of low wear regime of sliding friction.

A. Influence of surface roughness

The first and foremost issue is the reproducibility of the modeling results, namely it is about the interval of applied normal pressure σ_{Load} stability within which the low wear regime can exist. In other words, how sensitive is the σ_{crit} value with regard to randomization of the initial surface? Special investigations undertaken by us in this field have shown that this criterion stays constant given that integral initial roughness characteristics of both deformable and rigid surfaces (R_{max} , R_a , $R_{\text{max}}^{\text{rigid}}$, and R_a^{rigid}) are kept constant too. Furthermore, $W(t)$ dependencies in the catastrophic wear regime practically coincide with those shown in Fig. 2(a). More detailed information on this issue can be also found in the Supplemental Material [41]. Here we can state that an analogous conclusion will be also true for the PTE materials.

The results of this modeling testify that dry sliding wear behavior of NTE materials did not reveal any dependence on the initial surface roughness details. Hence another related question arises here about the effect of integral initial parameters of both deformable and rigid surface.

To answer this question, we carried out an additional study for different deformable surfaces, which were characterized

by different values of R_a (in all cases the ratio R_{max}/R_a was kept equal to 4 as in the above-considered reference system). The same rigid surface was used in all additional simulations. The modeling showed a linear $\sigma_{\text{crit}}(R_a)$ dependence as follows: $\sigma_{\text{crit}} = a - bR_a$. Let us note that such dependence is the weak one so that a twofold variation in R_a resulted in changing the σ_{crit} limited within 10%. Such a weak dependence between R_a and σ_{crit} may be related to the fact that initial roughness of the deformable surface is almost completely destroyed during the running-in stage.

The above statement is not true for the roughness of the rigid countersurface. Previously presented results were obtained using only one initial rigid countersurface roughness value, namely $R_a^{\text{rigid}} \approx 0.5 \mu\text{m}$. To study the effect of initial roughness on the transition from steady low to catastrophic wear (σ_{crit}) a number of experiments were carried out by varying R_a^{rigid} from zero to R_a (in all cases the ratio $R_{\text{max}}^{\text{rigid}}/R_a^{\text{rigid}}$ was the same as in the reference system). It was found out that the threshold stress decreased exponentially when increasing the roughness and such dependence may be adequately approximated by a function as follows: $\sigma_{\text{crit}} \sim B e^{-R_a^{\text{rigid}}/R_0}$, where B is the constant and R_0 is the normalization coefficient which can be expressed in terms of the deformable surface initial roughness R_a and equals $0.2\text{--}0.3 R_a$. For $R_a^{\text{rigid}} > 0.6\text{--}0.7 R_a$ the σ_{crit} is close to zero, i.e., no steady low wear regime is feasible. Such a result is provided by the fact that the number of contacts does not sufficiently increase at the running-in stage to decrease maximum values of contact stresses below the ultimate stress C . Therefore, the temperature-stimulated surface smoothing and steady low wear on NTE materials may be reduced to almost nothing unless the rigid abrading surface has low enough relative roughness.

B. Influence of thermally induced change of the contact area

Temperature-induced NTE material asperity geometry changes involve (a) asperity height Y reduction and (b) asperity real contact area S reduction. The first one is a fundamental factor of the worn surface roughness peaks leveling and, therefore, the feasibility of so-called wearless sliding (or sliding accompanied with negligible wear). The temperature-induced reduction of real contact area S must then produce the opposite effect of increasing contact pressure on the asperity and ensuing its enhanced wear.

To elucidate the effect of thermal change of asperity contact area we carried out an additional study using temperature-independent values of S ($\Delta S/\Delta T = 0$). It was shown that the σ_{Load} interval within which the wearless or low wear regime occurred (σ_{crit}) was increased by $\sim 40\%$ as compared to that obtained earlier using the approximation as follows: $S = S_0(1 + \alpha \Delta T)^2$. Furthermore, for temperature-independent value of asperity contact area, the wearless regime was found to exist in a wider R_a^{rigid} range even up to $R_a^{\text{rigid}} = R_a$. Let us remind that when using approximation (4), the maximum value of R_a^{rigid} to provide the low wear regime was about $0.7 R_a$.

Therefore, thermal shrinking of asperity height can be a governing factor for wear reduction, while thermal reduction of contact area may be an accompanying opposite action

factor to confine the occurrence of low wear regime. Also, this negative effect of the contact area reduction on the critical parameter σ_{crit} is the first order of smallness parameter as compared to the asperity height reduction.

The dependence (4) was assumed in modeling to account for proportional thermal shrinking of the asperity dimensions with retaining its conformity. Such an approximation can be considered as an upper bound of the contact area thermal shrinking magnitude. As shown, even with such a limiting approximation there is a wide enough applied normal pressure interval within which the low wear regime can occur.

Certain types and parameters of the functional dependence $S(T)$ are defined by an asperity geometry and lower-scale roughness of the top of asperities. In particular, the presented here model of a rough surface, as well as expressions (3) and (4) for temperature-induced expansion or shrinking, do not refer to some special asperity geometry but adequately approximate rectangular parallelepipeds or cylinders. Using more complex asperity shape approximations such as trapezoidal or ellipsoidal would plausibly result in a weaker or even opposite sign temperature dependence of the asperity contact area. That would lead both to an increasing σ_{crit} and roughness value interval of low wear regime existence up to $R_a^{\text{rigid}} > R_a$ at least for given mechanical and thermal-physical parameters of the material.

C. Dimensionless control parameters

Both mechanical and thermophysical properties of NTE material play a great role in governing the stability of wear. In particular, the threshold stress σ_{crit} , which corresponds to a transition from low to catastrophic wear in sliding on NTE material, is determined by a number of the material's thermal, physical, and mechanical characteristics. The general way of formalizing the effects of material parameters can be revealing of dimensionless parameters, which can be used to characterize the phenomenon. These control parameters combine the dimensional mechanical or thermophysical characteristics and loading variables. We revealed two (mechanical and thermophysical) dimensionless parameters, which control the border between low wear and catastrophic wear regimes for NTE materials.

Mechanical behavior of the modeled body's surface is first of all defined by Young's modulus E and ultimate strength C . Young's modulus determines the value of asperity stiffness $K \sim ES_0/D$ (D is the normalizing constant having length dimension) and defines the value of asperity strain in response to the applied contact stress. Reducing Young's modulus value results in increasing the number of contact spots thus reducing the maximum local contact stress. Increasing the E value, i.e., increasing the deformable surface's stiffness, provides the inverse effect. The ultimate stress C determines the ultimate strain of the asperity, the maximum normal load, which the surface can sustain without fracture of asperities, and finally the time-averaged number of contacts during friction. Consequently, threshold stress σ_{crit} should inversely depend on Young's modulus and directly depend on C . The simulation results show σ_{crit} is inversely proportional to E and directly proportional to C^2 . Therefore, it is possible now to define a dimensionless combination $M = \sigma_{\text{Load}}E/C^2$, which unambiguously

allows determining the threshold position between mild and catastrophic wear for NTE materials with different combinations of E and C and other material characteristics and loading rate kept equal. Low steady and catastrophic wear will be thus realized at $M < M_{\text{crit}}$ and $M > M_{\text{crit}}$, respectively.

The particular value of M_{crit} depends on the wear model parameters, i.e., on both H_w^{min} and $dH_w/d\sigma_{\text{eq}}$. It was shown in the modeling when keeping the $dH_w/d\sigma_{\text{eq}}$ quantity constant that $M_{\text{crit}}(H_w^{\text{min}})$ dependence is a decreasing one and may be adequately approximated using a linear function as follows: $M_{\text{crit}} = M_{\text{crit}}^0 - AH_w^{\text{min}}$. The characteristic scale of M_{crit}^0 is of the order of unity. Dependence $M_{\text{crit}}(dH_w/d\sigma_{\text{eq}})$ is also a decreasing function.

Thermophysical properties such as heat conductivity k and heat capacity c are very important for sliding dynamics on the NTE materials since all the above-described wear specifics are determined by an interplay between the heat release and removal processes. The relationship between k and c defines the asperity temperature dynamics at all wear stages thusly having its effect on the worn surface topography. Simulation results showed that increasing the heat conductivity by a factor of 10 provides more efficient heat removal and reducing the mean surface temperature by a factor of 1.5 resulted in the heat capacity kept constant. The reduced mean surface temperature leads to reducing the smoothing effect from the negative TEC. The threshold value M_{crit} is decreased by $\sim 15\%$. A twofold increase of the heat capacity value provides reducing the mean surface temperature by 15–20% while a dimensionless threshold M_{crit} value decreases within 10% analogously to that of heat conductivity k .

The higher the surface temperature, the greater the thermal shrinking of asperities and the more favorable conditions for the transition of friction into a low wear regime (keeping in mind that a stationary value of the surface temperature should be below the upper temperature limit of structural stability of the NTE material). The mean temperature on the contact surface is determined by the balance of heat release and heat removal rates. The former is characterized by friction heat release power $q = \mu \sigma_{\text{Load}}V_{\text{sl}}$, while the latter is effectively described by the heat flow $\nu = k(dT/dy)_{\text{surf}}$, where the lower index "surf" denotes temperature gradient near the surface (in a subsurface layer whose thickness Δy is equal to the asperity width Δx). A dimensionless combination $L = \nu/q \sim \sigma_{\text{Load}}V_{\text{sl}}/k(\Delta T/\Delta y)$, where ΔT is the temperature difference in the surface layer of thickness $\Delta y = \Delta x$, unambiguously allows determining the threshold position between the low wear and catastrophic wear regimes of friction for NTE materials. The special study showed that critical (threshold) value of the parameter $L(L_{\text{crit}})$, which is a boundary between the low steady wear regime ($L < L_{\text{crit}}$) and the catastrophic wear regime ($L > L_{\text{crit}}$), is approximately constant for NTE materials with different combinations of k and c and mechanical material characteristics kept equal. The introduced control parameter L is a thermophysical analogy of the well-known dimensionless Darcy number, which also reflects the balance of two competing processes (increase in the value of pore pressure due to mechanical straining of porous fluid-saturated material and decrease of pore pressure due to fluid flow in the pore space).

It should be noted that the value of temperature gradient $\Delta T/\Delta y$ in the definition of L can be roughly estimated using a solution of the trivial one-dimensional heat conduction problem with the von Neuman condition on one boundary (heat source of power $q = \mu \sigma_{\text{Load}} V_{\text{sl}}$) and the Dirichlet condition ($T = T_0$) on the other. A stationary temperature gradient at the distance $\Delta y = \Delta x$ from the source may be used as $\Delta T/\Delta y$ to define L . Also note that inertia thermophysical parameter c (heat capacity) is implicitly contained in the definition of L since it defines both surface temperature and temperature gradient $(dT/dy)_{\text{surf}}$.

V. CONCLUDING REMARKS

The results presented in this paper were obtained using an asperity contact model that can be related to a group of bearing-area (asperity-based) models. This type of model assumes a row of simplifications in describing the surfaces and contacting which make them considerably less accurate as compared to direct (“brute force”) computational models. In particular, the results of the recent benchmark contact problem resolved using different contact mechanics methods as well as other comparative studies demonstrate that the asperity-based models can be successfully used for qualitative estimation of the contact-patch size, gap, or interfacial (contact) stress distributions on the contact surface [42,43]. Corresponding quantitative estimations may, however, differ from those obtained using more accurate continuum mechanics models multiply.

This is “because bearing-area models predict contact patches to be too localized and therefore too large” [42]. Nev-

ertheless, asperity-based models are able to correctly describe stress peak distribution (although generally overestimate the compressive stress) and to reproduce the dependence of the effective contact area on load. That is why the asperity-based models are suitable for revealing qualitative dependences and so-called “control parameters” (and stimulating thinking and new ideas). So, the present work should be considered as qualitative research intended to understand trends rather than to produce accurate values.

We showed that frictional heating of the surface of NTE materials accompanied by temperature-induced smoothing and reduction of local contact pressures makes possible the implementation of steady low wear or even wearless friction at quite high applied normal loads. Such behavior is qualitatively different from that of PTE materials and may be related to a special type adaptation mechanism. The wear reduction effect of negative thermal expansion coefficient makes the NTE materials extremely attractive for applications in both low- and heavy-loaded tribological devices, for example as components of composite friction (brake) materials with PTE and NTE components. Controlling both mechanical and thermophysical characteristics of frictional composites, it is feasible to develop effective low or even zero wear rate tribocoupling.

ACKNOWLEDGMENT

The work was performed according to the Government research assignments for the Institute of Strength Physics and Materials Science of Siberian Branch Russian Academy of Sciences (ISPMS SB RAS), Projects No. III.23.1.4 and No. III.23.2.4.

-
- [1] D. Kuhlmann-Wilsdorf, *Mater. Sci. Eng.* **93**, 119 (1987).
 - [2] M. Kalin and J. Vizintin, *Wear* **249**, 172 (2001).
 - [3] E. H. Smith and R. D. Arnell, *Tribol. Lett.* **52**, 407 (2013).
 - [4] H. A. Abdel-Aal, in *Encyclopedia of Tribology*, edited by Q. J. Wang and Y. W. Chung (Springer, Boston, 2013).
 - [5] A. S. Iquebal, D. Sagapuram, and S. T. S. Bukkapatnam, *Sci. Rep.* **9**, 10617 (2019).
 - [6] S. K. Lee, R. Han, E. J. Kim, G. Y. Jeong, H. Khim, and T. Hirose, *Nat. Geosci.* **10**, 436 (2017).
 - [7] M. Umar, R. A. Mufti, and M. Khurram, *Tribol. Int.* **118**, 170 (2018).
 - [8] K. B. Jinesh, S. Yu. Krylov, H. Valk, M. Dienwiebel, and J. W. M. Frenken, *Phys. Rev. B* **78**, 155440 (2008).
 - [9] S. Yu. Krylov, K. B. Jinesh, H. Valk, M. Dienwiebel, and J. W. M. Frenken, *Phys. Rev. E* **71**, 065101(R) (2005).
 - [10] H. Spikes, *Friction* **6**, 1 (2018).
 - [11] N. L. Savchenko, Yu. A. Mirovoy, A. S. Buyakov, A. G. Burlachenko, M. A. Rudmin, I. N. Sevostyanova, S. P. Buyakova, and S. Yu. Tarasov, *Wear* **446–447**, 203204 (2020).
 - [12] A. A. Voevodin, C. Muratore, and S. M. Aouadi, *Surf. Coat. Technol.* **257**, 247 (2014).
 - [13] G. Cui, Y. Liu, S. Li, H. Liu, G. Gao, and Z. Kou, *Sci. Rep.* **10**, 6816 (2020).
 - [14] K. Takenaka, *Front. Chem. (Lausanne, Switz.)* **6**, 267 (2018).
 - [15] S. Abbasi, S. Teimourimanesh, T. Vernersson, U. Sellgren, U. Olofsson, and R. Lundén, *Wear* **314**, 171 (2014).
 - [16] J. R. Barber, *Proc. R. Soc. London, Ser. A* **312**, 381 (1969).
 - [17] J. R. Barber, *Wear* **10**, 155 (1967).
 - [18] Y. Meng, J. Xu, Z. Jin, B. Prakash, and Y. Hu, *Friction* **8**, 221 (2020).
 - [19] O. Hod, E. Meyer, Q. Zheng, and M. Urbakh, *Nature (London)* **563**, 485 (2018).
 - [20] J. Chen, L. Hu, J. Deng, and X. Xing, *Chem. Soc. Rev.* **44**, 3522 (2015).
 - [21] A. G. Akulichev, B. Alcock, A. Tiwari, and A. T. Echtermeyer, *J. Mater. Sci.* **51**, 10714 (2016).
 - [22] J. Ouyang, Y. Li, B. Chen, and D. Huang, *Materials* **11**, 748 (2018).
 - [23] N. C. Burtch, S. J. Baxter, J. Heinen, A. Bird, A. Schneemann, D. Dubbeldam, and A. P. Wilkinson, *Adv. Funct. Mater.* **29**, 1904669 (2019).
 - [24] J. Chen, Q. Gao, A. Sanson, X. Jiang, Q. Huang, A. Carnera, C. G. Rodriguez, L. Olivi, L. Wang, L. Hu, K. Lin, Y. Ren, Z. Lin, C. Wang, L. Gu, J. Deng, J. P. Attfield, and X. Xing, *Nat. Commun.* **8**, 14441 (2017).
 - [25] Q. Wang, J. A. Jackson, Qi Ge, J. B. Hopkins, C. M. Spadaccini, and N. X. Fang, *Phys. Rev. Lett.* **117**, 175901 (2016).
 - [26] M. T. Dove and H. Fang, *Rep. Prog. Phys.* **79**, 066503 (2016).
 - [27] J. P. Attfield, *Front. Chem. (Lausanne, Switz.)* **6**, 371 (2018).
 - [28] T. A. Mary, J. S. O. Evans, T. Vogt, and A. W. Sleight, *Science* **272**, 90 (1996).
 - [29] J. Li, S. Meng, L. Qin, and H. Lu, *Solid State Commun.* **247**, 58 (2016).

- [30] M. Ramzan, W. Luo, and R. Ahuja, *J. Appl. Phys.* **109**, 033510 (2011).
- [31] A. R. Hinkle, W. G. Nöhring, R. Leute, T. Junge, and L. Pastewka, *Sci. Adv.* **6**, eaax0847 (2020).
- [32] B. Weber, T. Suhina, T. Jungle, L. Pastewka, A. M. Brouwer, and D. Bonn, *Nat. Commun.* **9**, 888 (2018).
- [33] B. N. J. Persson, O. Albohr, U. Tartaglino, A. I. Volokitin, and E. Tosatti, *J. Phys.: Condens. Matter* **17**, R1 (2005).
- [34] K. Kato, *Wear* **241**, 151 (2000).
- [35] A. V. Dimaki, E. V. Shilko, I. V. Dudkin, S. G. Psakhie, and V. L. Popov, *Sci. Rep.* **10**, 1585 (2020).
- [36] R. Aghababaei, D. Warner, and J. Molinari, *Nat. Commun.* **7**, 11816 (2016).
- [37] R. Aghababaei, T. Brink, and J. F. Molinari, *Phys. Rev. Lett.* **120**, 186105 (2018).
- [38] J. von Lantz, L. Pastewka, P. Gumbsch, and M. Moseler, *Tribol. Lett.* **63**, 26 (2016).
- [39] A. I. Dmitriev, L. B. Voll, and V. L. Popov, *Wear* **458–459**, 203402 (2020).
- [40] A. I. Dmitriev, A. Yu. Smolin, V. L. Popov, and S. G. Psakhie, *Phys. Mesomech.* **12**, 11 (2009).
- [41] See Supplemental Material at <http://link.aps.org/supplemental/10.1103/PhysRevE.102.042801> for videos for understanding the dynamics of roughness change.
- [42] M. H. Müser, W. B. Dapp, R. Bugnicourt, P. Sainsot, N. Lesaffre, T. A. Lubrecht, B. N. J. Persson, K. Harris, A. Bennett, K. Schulze, S. Rohde, P. Ifju, W. G. Sawyer, T. Angelini, H. A. Esfahani, M. Kadkhodaei, S. Akbarzadeh, J.-J. Wu, G. Vorlaufer, A. Vernes, S. Solhjoo, A. I. Vakis, R. L. Jackson, Y. Xu, J. Streater, A. Rostami, D. Dini, S. Medina, G. Carbone, F. Bottiglione, L. Afferrante, J. Monti, L. Pastewka, M. O. Robbins, and J. A. Greenwood, *Tribol. Lett.* **65**, 118 (2017).
- [43] C. Campana, M. H. Muser, and M. O. Robbins, *J. Phys.: Condens. Matter* **20**, 354013 (2008).